Top-antitop and top-top resonances in the dilepton channel at the CERN LHC

Top-antitop and top-top resonances in the dilepton channel at the CERN LHC

Yang Bai[a] and Zhenyu Han[b]

[a] *Theoretical Physics Department, Fermi National Accelerator Laboratory,*
P.O. Box 500, Batavia, IL 60510, U.S.A.

[b] *Department of Physics, University of California,*
Davis, CA 95616, U.S.A.

E-mail: bai@fnal.gov, zhenyuhan@physics.ucdavis.edu

ABSTRACT: We perform a model-independent study for top-antitop and top-top resonances in the dilepton channel at the Large Hadtron Collider. In this channel, we can solve the kinematic system to obtain the momenta of all particles including the two neutrinos, and hence the resonance mass and spin. For discovering top-antitop resonances, the dilepton channel is competitive to the semileptonic channel because of the good resolution of lepton momentum measurement and small standard model backgrounds. Moreover, the charges of the two leptons can be identified, which makes the dilepton channel advantageous for discovering top-top resonances and for distinguishing resonance spins. We discuss and provide resolutions for difficulties associated with heavy resonances and highly boosted top quarks.

JHEP04(2009)056

Contents

1 Introduction

Being the unique standard model (SM) fermion with a mass of the electroweak symmetry breaking scale, the top quark may be closely related to the TeV scale new physics. In particular, many of the new physics candidates predict a $t\bar{t}$ (tt) resonance, i.e., a heavy particle that decays to $t\bar{t}$ (tt). The $t\bar{t}$ resonance occurs, for example, in Technicolor [1], Topcolor [2], Little Higgs [3], and Randall-Sundrum (RS) models [4], while the tt resonance exists in the grand unified theory in the warped extra-dimension [5]. Therefore, it is crucial to study $t\bar{t}$ (tt) invariant mass distributions and look for possible resonances at the ongoing Large Hadron Collider (LHC), which may provide us the opportunity for revealing the new physics beyond the SM .

The top quark almost only decays to a b quark and a W boson. Depending on how the W boson decays, events with a pair of tops can be divided to the all-hadronic, the semileptonic and the dilepton channels. The all-hadronic channel, in which both W's decay hadronically, has the largest branching ratio of 36/81, but suffers from the largest background since that all observed objects are jets. The semileptonic channel, in which one W decays hadronically and the other one decays leptonically, has a significant branching ratio of 24/81 and also smaller background. Although there is one neutrino in the event, only its longitudinal momentum is unknown, which can be easily extracted using the W mass constraint. Therefore, this has been thought to be the best channel for discovering $t\bar{t}$ resonance and most of existing studies have been concentrating on this channel [6–8]. The dilepton channel, in which both W's decay leptonically, has been thought to be a very challenging and not promising channel. The reason is twofold: first, not counting τ's,

the branching ratio for this channel is only 4/81; second, due to the fact that there are two neutrinos in the final states, the event reconstruction is much more difficult than the semileptonic channel.

Nevertheless, the dilepton channel also has its own merits, making it more than a complementary to the other two channels. An obvious advantage is that it has much smaller SM backgrounds. More importantly, the two leptons in the decay products carry information that is unavailable in the other channels. First, it is well-known that the charged lepton is the most powerful analyzer of the top spin [9, 10], because its angular distribution is 100% correlated with the top polarization in the top rest frame. The down-type quark from hadronic decay of the W boson has an equal power, but it is indistinguishable from the up-type quark in a collider detector. If the b jet from the top decay is not tagged, the ambiguity is even worse. Only the dilepton channel is free from this ambiguity.

Secondly, the charges of the two leptons are both measurable, which makes the same-sign dilepton channel ideal for studying tt or $\bar{t}\bar{t}$ production, since it has very small SM backgrounds. Note that although we are discussing resonances, the analysis applies equally for any events with two same-sign top quarks, as long as there are not missing particles other than the two neutrinos. For example, it can be used to study the excess of tt or $\bar{t}\bar{t}$ production in flavor violating processes [11–13]. On the contrary, the charge information in the other two channels is unavailable,[1] and hence a more significant event rate is needed to see an excess over the SM $t\bar{t}$ background.

Motivated by the above observations, we perform a model independent study on $t\bar{t}$ (tt) resonances in the dilepton channel. The crucial step of this analysis is the event reconstruction, which we describe in the next section. We will focus on the most challenging case when the resonance is heavy (≥ 2 TeV) and discuss a few related difficulties and their solutions. As an illustration, the method is applied to a KK gluon in the RS model with a mass of 3 TeV. In section 3, we estimate the discovery limits of representative resonances with different spins. It is shown that despite the smaller branching ratio, the discovery limits from this channel compete with those from the semileptonic channel. In section 4, we present the method for spin measurements and estimate the minimal number of events needed to distinguish the spin of the resonance. Section 5 contains a few discussions and the conclusion.

2 Event reconstruction

2.1 The method

In this section, we discuss the method for reconstructing the $t\bar{t}$ system in the dilepton channel at the LHC. The process we consider is $pp \to \Pi \to t\bar{t} \to b\bar{b}W^+W^- \to b\bar{b}\ell^+\ell^-\nu_\ell\bar{\nu}_\ell$, with Π a $t\bar{t}$ resonance and $\ell = e, \mu$. There can be other particles associated with the Π production such as the initial state radiation, but in our analysis it is crucial that the missing momentum is only from the two neutrinos. The method described in this section can also be applied to tt resonances.

---

[1]It is possible to identify the charges of the b-jets but only at a few percent level.

Assuming tops and W's are on-shell and their masses are known, the 4-momenta of the neutrinos can be solved from the mass shell and the measured missing transverse momentum constraints [14]:

$$
\begin{aligned}
p_\nu^2 = p_{\bar\nu}^2 &= 0 \,, \\
(p_\nu + p_{l+})^2 = (p_{\bar\nu} + p_{l-})^2 &= m_W^2 \,, \\
(p_\nu + p_{l+} + p_b)^2 = (p_{\bar\nu} + p_{l-} + p_{\bar b})^2 &= m_t^2 \,, \\
p_\nu^x + p_{\bar\nu}^x = \not{p}^x, \qquad p_\nu^y + p_{\bar\nu}^y &= \not{p}^y \,,
\end{aligned}
\qquad (2.1)
$$

where p_i is the four-momentum of the particle i. We have 8 unknowns from the two neutrinos' four-momenta and 8 equations. Therefore, eqs. (2.1) can be *solved* for discrete solutions. This system can be reduced to two quadratic equations plus 6 linear equations [15, 16]. In general, the system has 4 complex solutions, which introduces an ambiguity when more than one solutions are real and physical. After solving for p_ν and $p_{\bar\nu}$, it is straightforward to obtain p_t and $p_{\bar t}$ and calculate the $t\bar t$ invariant mass $M_\Pi^2 = (p_t + p_{\bar t})^2$.

The system in eqs. (2.1) has been applied to measure the top mass [14, 17] and to study the spin correlations in $t\bar t$ decays [17, 18]. These studies focus on low center of mass energies below 1 TeV and involve only the SM $t\bar t$ production. We will concentrate on the heavy-resonance case when t, $\bar t$ and their decay products are highly boosted. There are a few complications in disentangling new physics contributions from the SM, as discussed below.

The first complication comes from the fact that for a highly boosted top, its decay products are collimated and therefore are difficult to be identified as isolated objects. In other words, all decay products of the top, in either the hardronic or the leptonic decay channels, form a fat "top jet". This interesting fact has triggered recent studies for developing new methods to distinguish top jets from ordinary QCD jets [19, 20]. For the dilepton channel, in order to keep as many signal events as possible, we include both isolated leptons and non-isolated muons. Non-isolated muons can be measured in the muon chamber, while non-isolated electrons are difficult to be distinguished from the rest of the jet and therefore not included in our analysis. This is very different from the low center-of-mass energy case where two isolated leptons can often be identified.

Once non-isolated muons are included, we have to consider the SM non-$t\bar t$ backgrounds such as bt and bb productions with one or two muons coming from b or c hadron decays. Since muons from hadronic decays are relatively softer, we will use a high $p_T > 100$ GeV cut for the non-isolated muons to reduce the background. This is similar to using the jet energy fraction carried by the muon as a cut [19]. Similarly, it is unnecessary to require one or two b-jet taggings, which may have a small efficiency at high energies [21]. Instead, we consider all signal and background events with two high-p_T jets. Besides high-p_T cuts, the mass-shell constraints in eqs. (2.1) are also efficient for reducing the background/signal ratio.

The second complication is caused by wrong but physical solutions. Part of the wrong solutions come from wrong combinatorics — either one or more irrelevant jets or leptons from sources other than $t\bar t$ are included in the reconstruction equations, or the relevant jets and leptons are identified but combined in a wrong way. Even when we have identified the correct objects and combinatorics, there can be wrong solutions due to the non-linear nature

of the equation system. As mentioned before, there could be up to three wrong solutions in addition to the correct one. The wrong solutions will change the $t\bar{t}$ invariant mass distribution. This is not a severe problem for a light ($< 1\,\mathrm{TeV}$) resonance because both signals and backgrounds can be large. The wrong solutions will smear but not destroy the signal peak. For heavy resonances in the multi-TeV range, the signal cross section is necessarily small due to the rapid decreasing of the parton distribution functions (PDF's). This would not be a problem if we only obtained the correct solution since the decreasing would happen for both the signals and the backgrounds. However, when a wrong solution is present, it will shift the $t\bar{t}$ invariant mass to a different value from the correct one, either lower or higher. Due to the large cross section of the SM $t\bar{t}$ production in the low invariant mass region, even if a small fraction of masses are shifted to the higher region, the signal will be swamped.

Wrong solutions exist because the momenta of the neutrinos are unknown except the sums of their transverse momenta. Clearly, for a $t\bar{t}$ invariant mass shifted to be higher than the correct value, the solved neutrino momenta are larger than their right values statistically. Therefore, we can reduce the fraction of wrong solutions by cutting off solutions with unnaturally large neutrino momenta. This is achieved by two different cuts. First, we can cut off "soft" events before reconstruction. That is, we apply a cut on the cluster transverse mass $m_{T_{\mathrm{cl}}}$ defined from the measured momenta [7]:

$$m_{T_{\mathrm{cl}}}^2 = \left(\sqrt{p_T^2(l^+ l^- b\bar{b}) + m^2(l^+ l^- b\bar{b})} + \not{p}_T \right)^2 - \left(\vec{p}_T(l^+ l^- b\bar{b}) + \vec{\not{p}}_T \right)^2, \qquad (2.2)$$

where $\vec{p}_T(l^+l^-b\bar{b})$ and $m^2(l^+l^-b\bar{b})$ are the transverse momentum and the invariant mass of the $l^+l^-b\bar{b}$ system, and $\not{p}_T = |\vec{\not{p}}_T|$. Second, after reconstruction, we define a cut on the fraction of the transverse momentum carried by the neutrinoes,

$$r_{\nu b} = \frac{p_T^\nu + p_T^{\bar\nu}}{p_T^b + p_T^{\bar{b}}} < 2. \qquad (2.3)$$

As we will see in section 2.3, the $r_{\nu b}$ cut is useful for increasing signal/background ratio. The value in eq. (2.3) is approximately optimized for the examples we consider and taken to be fixed in the rest of the article. On the other hand, we choose to explicitly vary the $m_{T_{\mathrm{cl}}}$ cut to optimize the discovery significance because it is what the significance is most sensitive to. In practice, one could as well optimize all other cuts and obtain better results.

The third issue is with regard to the experimental resolutions. The smearing of the measured momenta modifies the coefficients in eqs. (2.1). When the modification is small, the correct solutions of the neutrino momenta are shifted, but we still obtain real solutions.[2] However, when the modification is large, it is possible to render the solutions to be complex. Again, this effect is more significant when the top is more energetic. The absolute smearings are larger (although the fractional resolution is better), which make it harder to have real solutions . For comparison, 38% signal events from a $1\,\mathrm{TeV}$ resonance have real solutions. The percentage decreases to 26% for a $3\,\mathrm{TeV}$ resonance. This is based on a semi-realistic analysis detailed in the next subsection.

---

[2]Note that the finite widths of the top quark and the W boson have similar effect, although their $1-2\,\mathrm{GeV}$ widths are negligible compared with the detector resolutions.

The best treatment of this problem is perhaps to find the real solutions by varying the visible momenta, and then weight the solutions according to the experimental errors. In this article, we adopt a much simpler solution, namely, we keep those solutions with a small imaginary part. More precisely, we first solve eqs. (2.1) for p_ν and $p_{\bar\nu}$. Then we keep all four complex solutions and add them to the corresponding lepton and b-jet momenta to obtain p_t and $p_{\bar t}$. We demand

$$|\mathrm{Im}(E_t)| < 0.4\,|\mathrm{Re}(E_t)|\,, \quad |\mathrm{Im}(E_{\bar t})| < 0.4\,|\mathrm{Re}(E_{\bar t})|\,. \tag{2.4}$$

where E_t and $E_{\bar t}$ are respectively the energies of t and $\bar t$. Similar to the $r_{\nu b}$ cut, the values we choose in eq. (2.4) are approximately optimized and taken to be fixed through the rest of the article. For events passing the above cuts, we make the 4-momenta of t and $\bar t$ real by taking the norm of each component, but keep the sign of the original real part. Note that complex solutions always appear in pairs, giving the same real solution after taking the norm. We only count it once.

2.2 Event generation

The hard process of $pp \to \Pi \to t\bar t \to b\bar b\ell^+\ell^-\nu_\ell\bar\nu_\ell$ is simulated with TopBSM [22] in MadGraph/MadEvent [25], where Π denotes the $t\bar t$ resonance. In this article, we will consider a spin-0 color-singlet scalar, a spin-0 color-singlet pseudo-scalar, a spin-1 color octet and a spin-2 color-singlet. The major SM background processes, including $t\bar t$, $b\bar b$, $c\bar c$, $bb\ell\nu$ and $jj\ell\ell$, are also simulated with MadGraph/MadEvent using CTEQ6L1 PDF's [26]. We choose the renormalization and factorization scales as the square root of the quadratic sum of the maximum mass among final state particles, and p_T's of jets and massless visible particles, as described in MadGraph/MadEvent. Showering and hadronization are added to the events by Pythia 6.4 [27]. Finally, the events are processed with the detector simulation package, PGS4 [28]. We have not included theoretical uncertainties in the cross-section calculations, which mainly comes from PDF uncertainties at high invariant mass [22]. In ref. [22] (figure 3), it is estimated using the CTEQ6 PDF set that the SM $t\bar t$ cross-section has a theoretical uncertainty around 20%∼ 30% at 2 TeV, increasing to about 80% at 4 TeV, which may significantly affect some of the results in our analysis. Nevertheless, we note that the PDFs can be improved with the Tevatron data [29] at large x, and our focus here is event reconstruction. Therefore, we ignore systematic errors in the following discussions.

The cuts used to reduce the background/signal ratio are summarized below, some of which have been discussed in the previous section:

1. Before reconstruction

   - At least two leptons satisfying: $p_T > 20$ GeV for isolated leptons or $p_T > 100$ GeV for non-isolated muons. The two highest p_T leptons are taken to be the leptons in eqs. (2.1);
   - $m_{\ell\ell} > 100$ GeV where $m_{\ell\ell}$ is the invariant mass of the two highest p_T leptons.

- At least two jets satisfying: $p_T > 50$ GeV for b-tagged, $p_T > 150$ GeV for not-b-tagged. The two highest p_T jets are taken to be the b jets in eqs. (2.1);

- $\not{p}_T > 50$ GeV;

- Varying $m_{T_{\mathrm{cl}}}$ cut.

2. After reconstruction

- $|\mathrm{Im}(E_t)| < 0.4\,|\mathrm{Re}(E_t)|\,,\quad |\mathrm{Im}(E_{\bar{t}})| < 0.4\,|\mathrm{Re}(E_{\bar{t}})|\,;$

- $r_{\nu b} < 2\,.$

The complex solutions are made real using the method discussed in the previous section. There can be 0-4 solutions after the above cuts. We discard events with zero solution. For a solvable event with $n \geq 1$ solutions, we weight the solutions by $1/n$.

2.3 KK gluon as an example

We illustrate the efficiency of the reconstruction procedure by considering the KK gluon in the basic RS model with fermions propagating in the bulk. The KK gluon is denoted by Π_o^1, which has the following couplings to the SM quarks,

$$g_{L,R}^q = 0.2\,g_s\,,\quad g_L^t = g_L^b = g_s\,,\quad g_R^t = 4\,g_s\,,\quad g_R^b = -0.2\,g_s\,, \qquad (2.5)$$

where g_s is the strong coupling constant and q represents quarks in the light two generations. With this set of couplings, the KK gluon has a width $\Gamma_{\Pi_o^1} = 0.153\,M_{\Pi_o^1}$, and the branching ratio $Br(\Pi_o^1 \to t\,\bar{t}) = 92.6\%$. For a KK gluon of mass $3\,\mathrm{TeV}$, the total leading-order cross section in the dilepton channel is approximately $10\,\mathrm{fb}$. The parton level $m_{t\bar{t}}$ distribution is shown in figure 1, together with the SM $t\,\bar{t}$ background, also in the dilepton channel. The interference between the KK gluon and the SM is small and ignored in figure 1. Within the mass window $(M_G - \Gamma_G, M_G + \Gamma_G) \approx (2500, 3500)$ GeV, the total number of events is around 770 for the signal and 610 for the background, for $100\,\mathrm{fb}^{-1}$.

Although the SM $t\,\bar{t}$ production in the dilepton channel comprises the largest background, we have to consider backgrounds from other sources since we are utilizing not-b-tagged jets and non-isolated leptons, which can come from heavy flavor hadron decays. The major additional backgrounds are:

1. $t\,\bar{t}$ processes in other decay channels, which include the semi-leptonic channel, the all-hadronic channel and channels involving τ's;

2. Heavy flavor di-jets, including $b\bar{b}$ and $c\bar{c}$ with $b\bar{b}$ dominating;

3. Other processes that contain one or more isolated leptons including $jj\ell\ell$, $bb\ell v$ productions.

The above backgrounds are included in our particle level analysis. In table 1, we show the number of events of the signal and backgrounds before and after the reconstruction procedure. The cuts discussed in the previous subsection are applied, with a moderate
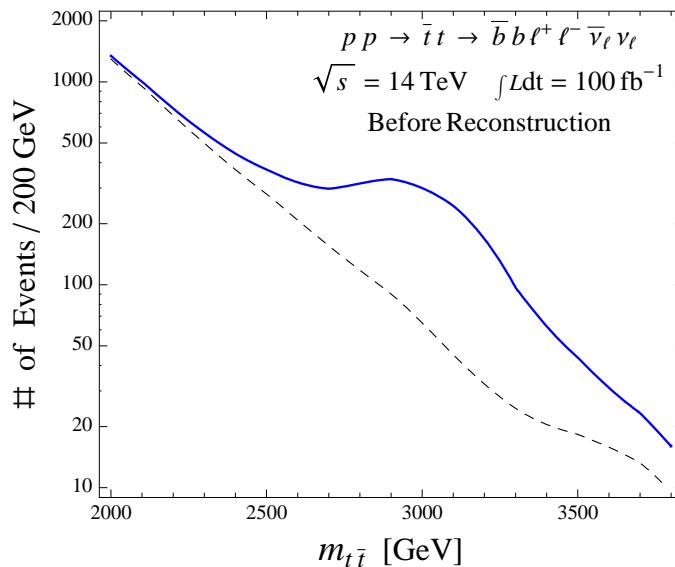
– 6 –

Figure 1. The number of events in the dilepton channel of the $t\bar{t}$ production through a KK gluon at the LHC. The mass and width of the KK gluon are chosen to be 3 TeV and 459 GeV, respectively. The solid (blue) curve is signal+background and the dashed (black) curve is the SM $t\bar{t}$ dilepton background.

	3 TeV KK gluon	$t\bar{t}$ dilep	$t\bar{t}$ others	$b\bar{b}$, $c\bar{c}$	$jj\ell\ell, bb\ell v$
Before Recon.	167	317	96	68	63
After Recon.	82	159	37	33	13
$r_{\rm vb} < 2$	73	146	31	7	11

Table 1. Number of signal and background events for 100 fb^{-1} before and after reconstruction.

$m_{T_{\rm cl}} > 1500\,{\rm GeV}$ cut. Note that these numbers are without any mass window cut, while the kinematic cuts in the previous subsection have been applied. Also note that the number of signal events is much smaller after detector simulation and applying the kinematic cuts: this is because most of the leptons are non-isolated when the $t\bar{t}$ resonance mass is as high as 3 TeV, and we have only included non-isolated muons in the analysis. The probability for both leptons from W decays to be muons is only $1/4$. This fact, together with the kinematic cuts, drastically reduces the number of signal events. This reduction also occurs for the SM $t\bar{t}$ dilepton events with a high center of mass energy.

From table 1, we can see the effects of the event reconstruction. Before applying the $r_{\nu b}$ cut, the reconstruction efficiencies for the signal events and the SM $t\bar{t}$ dilepton events are approximately equal and around 50%. The efficiencies for the other backgrounds are substantially smaller. Moreover, the cut on the variable $r_{\nu b}$, which is only available *after* the event reconstruction, also favors the signal and the SM $t\bar{t}$ dilepton events. Therefore, we obtain a larger S/B at the cost of slightly decreasing significance $S/\sqrt{B}$. In the following, we will define the significance after the event reconstruction.
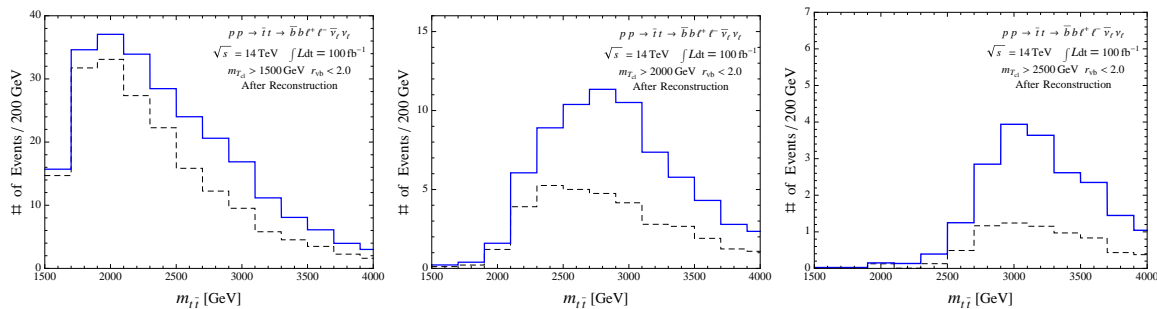
Figure 2. The event distributions of $t\bar{t}$ invariant masses after reconstruction. The solid (blue) histogram is signal+background and the dashed (black) histogram is background only. From left to right, we have the cuts on $m_{T_{cl}}$ to be 1500, 2000, 2500 GeV.

Of course, the effects of event reconstruction are beyond simple event counting. More importantly, we obtain the 4-momenta of the top quarks, which are necessary for determining the spin of the $t\bar{t}$ resonance. We will discuss the spin measurement in section 4. We also obtain the mass peak on top of the background after reconstruction, as can be seen from figure 2, where we show the $m_{t\bar{t}}$ distributions of both background and signal+background for a few different $m_{T_{cl}}$ cuts. For the left plot with $m_{T_{cl}} > 1500$ GeV, there is a clear excess of events, although the mass peak is not obvious. By comparing with figure 1, we see that S/B is smaller than the parton level distribution in the mass window (2500, 3500) GeV $\approx (M_G - \Gamma_G, M_G + \Gamma_G)$. This indicates that wrong solutions from the lower $m_{t\bar{t}}$ background events have contaminated the higher $m_{t\bar{t}}$ distribution. As we increase the $m_{T_{cl}}$ cut, the numbers of both signal events and background events decrease, but S/B is increasing, showing that the contamination is reduced. The contamination reduction is also confirmed by tracing back the reconstructed $m_{t\bar{t}}$ to its Monte Carlo origin. For the $m_{T_{cl}}$ cut of 1500 GeV, the reconstructed background $m_{t\bar{t}}$ in the mass window of (2500, 3500) GeV is decomposed as: 44% from the SM $t\bar{t}$ events with original $m_{t\bar{t}}$ smaller than 2500 GeV; 25% from the SM $t\bar{t}$ events with original $m_{t\bar{t}}$ larger than 2500 GeV; the other 21% come from other SM backgrounds. The decomposition becomes (in the same order as above) {23%, 43%, 34%} for the $m_{T_{cl}}$ cut of 2000 GeV, and {13%, 60%, 27%} for the $m_{T_{cl}}$ cut of 2500 GeV. Nevertheless we cannot choose too high a $m_{T_{cl}}$ cut since it can reduce $S/\sqrt{B}$. For the KK gluon example, the significance is maximized when the $m_{T_{cl}}$ cut is around 2000 GeV. More precisely, in the mass window (2500, 3500) GeV for M_G, we have $S/B = 0.69, 1.3, 1.8$ and $S/\sqrt{B} = 4.9, 6.1, 4.5$ for $m_{T_{cl}} \geq 1500, 2000, 2500$ GeV, respectively.

3 Discovery limits

Having discussed our strategy of selecting cuts to optimize the discovery limit, we now consider the needed signal cross section for different $t\bar{t}$ and tt resonances at 5σ confidence level (CL) at the LHC.

3.1 Statistics

We are interested in heavy resonances with masses from 2 to 4 TeV. In order to cover most of the signal events, we examine reconstructed masses in the range of $1.5 - 5.1$ TeV. We ignore uncertainties from the overall normalization of the signal and background cross sections, which can be determined from the low $m_{t\bar{t}}$ mass events, where the statistics is much better. To utilize the shape differences, we equally divide the mass range to $N_{\rm bin} = 18$ bins, which amounts to having a 200 GeV bin width. In each bin, we define the number of the background events as b_i, while the number of the signal events as s_i. When the number of events is small, the distribution is Poisson. Following [30], we first calculate the Pearson's χ^2 statistic

$$\chi^2 = \sum_i^{N_{\rm bin}} \frac{(n_i - v_i)^2}{v_i} = \sum_i^{N_{\rm bin}} \frac{s_i^2}{b_i}, \tag{3.1}$$

where $n_i = b_i + s_i$ is the measured value and $v_i = b_i$ is the expected value. Assuming that the goodness-of-fit statistic follows a χ^2 probability density function, we then calculate the p-value for the "background only" hypothesis

$$p = \int_{\chi^2}^{\infty} \frac{1}{2^{N_{\rm bin}/2}\,\Gamma(N_{\rm bin}/2)}\, z^{N_{\rm bin}/2-1}\, e^{-z/2}\, dz\,, \tag{3.2}$$

where $N_{\rm bin}$ counts the number of degrees of freedom. For a $5\,\sigma$ discovery, we need to have $p = 2.85 \times 10^{-7}$ and therefore $\chi^2 \approx 65$ for $N_{\rm bin} = 18$.

For a particular resonance, we define a reference model with a known cross section. We then vary the $m_{T_{\rm cl}}$ cut from 1.5 TeV to 3.5 TeV in 100 GeV steps to generate different sets of b_i and s_i. We find the optimized $m_{T_{\rm cl}}$ cut that maximizes the χ^2. After optimizing the $m_{T_{\rm cl}}$ cut, we multiply the number of signal events by a factor of Z to achieve $\chi^2 = 65$ or $5\,\sigma$ discovery. This is equivalent to requiring the production cross section of the signal to be Z times the reference cross section.

3.2 Discovery limits

For $t\bar{t}$ resonances, we choose a representative set of $t\bar{t}$ resonances with different spins and quantum numbers under SU(3) color gauge group. We label spin-0 color-singlet scalar, spin-0 color-singlet pseudo-scalar, spin-1 color octet and spin-2 color-singlet particles as Π^0, Π_p^0, Π_o^1 and Π^2 respectively. For the spin-0 particles, Π^0 and Π_p^0, we assume that they only couple to top quarks with couplings equal to the top Yukawa coupling in the standard model, and hence they are mainly produced through the one-loop gluon fusion process at the LHC. Their decay widths are around $3/(16\,\pi)$ times their masses and calculated automatically in the Madgraph. For the spin-one particle, Π_o^1, we still use the KK gluon described in section 2.3 as the reference particle, and use the same couplings defined in eq. (2.5). The decay width of the KK gluon is fixed to 0.153 times its mass. For the spin-two particle, Π^2, we choose the first KK graviton in the RS model as the reference particle, and choose the model parameter, $\kappa/M_{\rm pl} = 0.1$, where $M_{\rm pl}$ is the Planck scale and κ is defined in [4]. Its decay width is calculated in Madgraph.

For tt resonances, we study the spin-one particle, which is suggested to exist at the TeV scale in grand unified models in a warped extra-dimension [5]. Under the SM gauge symmetries, the X gauge boson is the up part of the gauge bosons with the quantum numbers $(\bar{3}, 2, 5/6)$. It has the electric charge $4/3$ and couples to up-type quarks with a form $g_i \, \epsilon_{abc} \, \bar{u}_{iL}^{\mathcal{C} \, a} \, \overline{X}_\mu^b \, \gamma^\mu \, u_{iL}^c \, + \, h.c.$ (i is the family index; a, b, c are color indices; $\mathcal{C}$ denotes charge conjugate). In general, the gauge couplings g_i depend on the fermion localizations in the fifth warped extra-dimension. However, we do not specify any details of model buildings including how to suppress the proton decay, and only focus on the discovery feasibility at the LHC. For simplicity, we model the tt resonance the same way as the KK gluon, but flip the sign of one lepton at the parton level. We also choose the reference tt production cross section through X as the cross section of $t\bar{t}$ production through the KK gluon described in eq. (2.5). We fix the decay width of X to be 10% of its mass. In our analysis, we use the same set of background events as in the $t\bar{t}$ case. There are two main sources of the SM backgrounds for same-sign dileptons. The lepton charges from b-jets can have either sign. Another source is lepton charge misidentifications. There are other intrinsic SM backgrounds from processes like $u \, \bar{d} \to W^+ W^+ d \, \bar{u}$. However, this is a pure electroweak process and hard to pass the reconstruction cuts. We neglect such processes in our analysis.

In figure 3, we show values of the multiplying factor Z for the $t\bar{t}\,(tt)$ production cross sections to have $5\,\sigma$ discovery at the LHC for 100 fb^{-1} integrated luminosity. Note that we do not change the widths of the resonances according to the models described above when multiplying the factor Z. Those models serve as reference points only. In obtaining the discovery limits, we have ignored all interferences between the resonances and the SM $t\bar{t}$ productions. As shown in ref. [22], the interference between a KK gluon or a KK graviton and the SM $t\bar{t}$ productions is negligible. For a spin-0 resonance (scalar or pseudo-scalar), a peak-dip structure in the $m_{t\bar{t}}$ distribution is generally visible at the parton level if the resonance is produced through gluon fusion similar to the SM Higgs. We do not anticipate that the interference will change our results significantly.

The discovery limits for the KK gluon are $3.2\,\mathrm{TeV}$ and $3.7\,\mathrm{TeV}$ for 100 fb^{-1} and 300 fb^{-1} integrated luminosity. For comparison, the discovery limit for the KK gluon in the semileptonic channel is $3.8\,\mathrm{TeV}$ for 100 fb^{-1} and $4.3\,\mathrm{TeV}$ for 300 fb^{-1} given in [8]. There they combine the invariant mass and top p_T distributions. If only the invariant mass distribution were used, the discovery limit would be reduced by a few hundred GeV. Therefore, the discovery limit in the dilepton channel is competitive to the semileptonic channel. Comparing the black (solid) line and the orange (thick dashed) line, we have a better discovery limit for the tt resonance than the $t\bar{t}$ resonance when they have the same production cross section. This is because the SM background for tt is much smaller than the background for $t\bar{t}$. The X gauge boson can be discovered with a mass up to $4.0\,\mathrm{TeV}$ and $4.4\,\mathrm{TeV}$, respectively, for 100 fb^{-1} and 300 fb^{-1}.

If a $t\bar{t}$ resonance is discovered, it is important to measure the mass. The peak position of the $m_{t\bar{t}}$ distribution in general does not coincide with the true resonance mass, and also shifts according to the $m_{T_{\mathrm{cl}}}$ cut applied, as can be seen in figure 2. We can eliminate this systematic error, as well as minimize the statistical error by using the usual "template" method. That is, we can generate the $m_{t\bar{t}}$ distributions for different input masses, and then
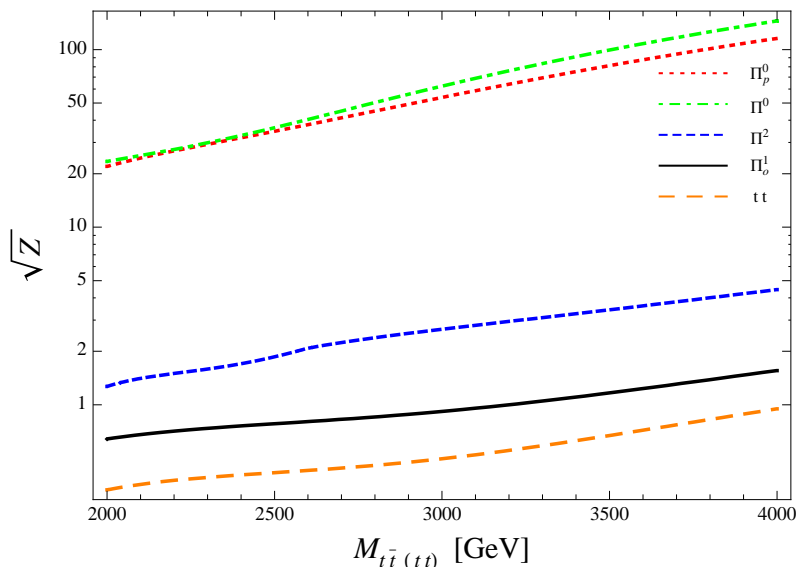
Figure 3. The multiplying factor Z (shown in the figure is its square root) for the production cross sections to have $5\,\sigma$ discovery at the LHC with a 100 fb^{-1} integrated luminosity, as a function of $t\bar{t}(tt)$ invariant masses. Π^0, Π^0_p, Π^1_o and Π^2 are spin-0 color-singlet scalar, spin-0 color-singlet pseudo-scalar, spin-1 color octet and spin-2 color-singlet $t\bar{t}$ resonances, respectively.

compare them with the measured distribution to obtain the true mass. A detailed study of mass measurement is beyond the scope of this article.

4 Spin measurements

The momenta of all particles are known after event reconstructions, which allows us to determine the spins of the $t\bar{t}$ resonances. We first consider the angular distributions of the top quark in the $t\bar{t}$ resonance rest frame. To minimize the effect of initial state radiation, we use the Collins-Soper angle [31] defined as the angle between the top momentum and the axis bisecting the angle between the two incoming protons, all in the $t\bar{t}$ rest frame. In the case that the initial state radiation vanishes, this angle becomes the angle between the top momentum and the beam direction. Using the lab frame momenta, the Collins-Soper angle is conveniently given by

$$\cos\theta = \frac{2}{m_{t\bar{t}}\sqrt{m_{t\bar{t}}^2 + p_T^2}}(p_t^+ \, p_{\bar{t}}^- - p_t^- \, p_{\bar{t}}^+), \tag{4.1}$$

where $m_{t\bar{t}}$ and p_T are the invariant mass and the transverse momentum of the $t\bar{t}$ system and $p_t^{\pm}$, $p_{\bar{t}}^{\pm}$ are defined by

$$p_t^{\pm} = \frac{1}{\sqrt{2}}(p_t^0 \pm p_t^z)\,, \quad p_{\bar{t}}^{\pm} = \frac{1}{\sqrt{2}}(p_{\bar{t}}^0 \pm p_{\bar{t}}^z)\,. \tag{4.2}$$

One can also consider angular correlations among the decay products of top quarks. As mentioned in the introduction, the best analyzer for the top polarization is the charged
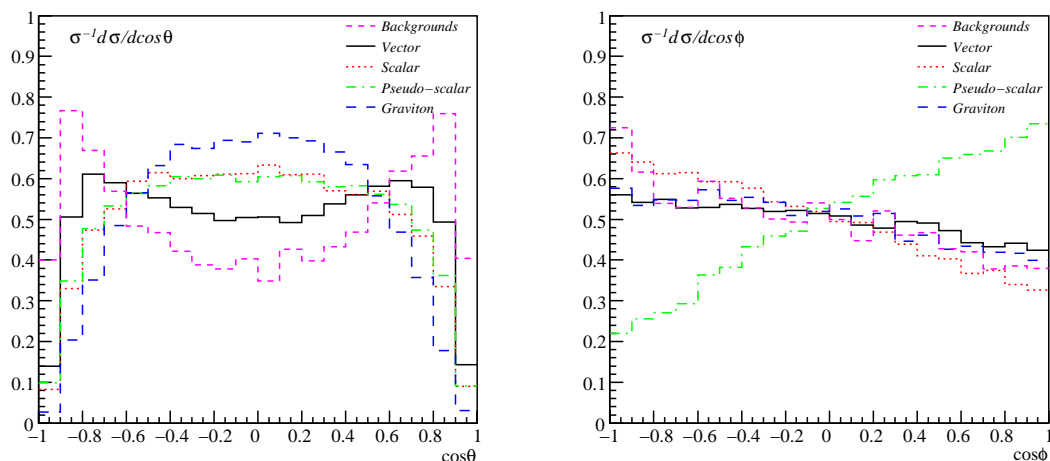
Figure 4. Distributions of the Collins-Soper angle θ (left) and the opening angle ϕ (right) at particle level for different resonances with a mass of $2\,\mathrm{TeV}$ and the SM backgrounds. A mass window cut $(1600\,\mathrm{GeV}, 2400\,\mathrm{GeV})$ is applied on all solutions.

lepton. Therefore, we examine the opening angle ϕ between the ℓ^+ direction in the t rest frame and the ℓ^- direction in the $\bar{t}$ rest frame. The parton level distribution for the opening angle has a form

$$\frac{1}{\sigma}\frac{d\sigma}{d\cos\phi} = \frac{1}{2}(1 - D\cos\phi)\,, \tag{4.3}$$

where D is a constant depending on the $t\bar{t}$ polarizations, and hence model details. At particle level, the distribution is affected by the experimental resolutions and wrong solutions from event reconstructions. In figure 4, we show the particle level distributions of $\cos\theta$ and $\cos\phi$ for 4 different $t\bar{t}$ resonances: a scalar, a pseudo-scalar, a vector boson that couples to left- and right-handed quarks equally, and a KK graviton in the RS model. The cuts described in section 2.2 are applied with $m_{T_{\mathrm{cl}}} > 1500\mathrm{GeV}$. A mass window cut of $(1600\,\mathrm{GeV}, 2400\,\mathrm{GeV})$ is also applied on the solutions to increase S/B. From the left panel of figure 4, we see significant suppressions in the forward and backward regions of $\cos\theta$, due to the kinematic cuts. Except that, both the scalar and the pseudo-scalar have a flat distribution in $\cos\theta$ and are hard to be distinguished from each other. The $\cos\theta$ distributions for the vector boson and the graviton show the biggest difference with respect to each other. As shown in the right panel of figure 4, the slope of the pseudo-scalar distribution in $\cos\phi$ has an opposite sign to all others, which can be used to identify a pseudo-scalar resonance. Therefore one has to use both distributions to distinguish the four particles.

Given the distributions, we can estimate how many events are needed to determine the spin of a $t\bar{t}$ resonance. We first reform the question in a more specific way: given experimentally observed distributions in $\cos\theta$ and $\cos\phi$ generated by a particle of spin s_a, we ask how many events are needed to decide, at 95% CL, that they are not from a particle of spin s_b. This is being done by comparing the observed distributions with Monte Carlo distributions of different spins. If the observed distributions are inconsistent with all

$s_a \backslash s_b$	Vector	Scalar	Pseudo-scalar	Graviton
Vector	-	661 (501)	262 (140)	316 (122)
Scalar	705 (577)	-	199 (94)	771 (455)
Pseudo-scalar	275 (182)	200 (116)	-	240 (128)
Graviton	356 (243)	878 (694)	239 (123)	-

Table 2. Number of *signal* events after reconstruction needed to distinguish a particle of spin s_a from spin s_b at 95% CL. The number of background events is fixed to 136, corresponding to 100 fb^{-1} data. All resonance masses are 2 TeV. For reference, the needed numbers of signal events without background are given in the parentheses.

but one spin, we claim that we have identified the spin. Of course, without real data, the "observed" distribution in this article is also from Monte Carlo. We quantify the deviation of two distributions from different spins s_a and s_b as

$$\chi^2_{s_a:s_b} = \sum_i^{N_{\mathrm{bin}}} \frac{(n_{s_a,i} - n_{s_b,i})^2}{n_{s_b,i}}, \qquad (4.4)$$

where N_{bin} is the total number of bins and is equal to 20 by choosing a 0.1 bin size for both $\cos\theta$ and $\cos\phi$; $n_{s_a,i}$ and $n_{s_b,i}$ are the number of events in the i'th bin, which satisfy $\sum n_{s_a,i} = \sum n_{s_b,i}$. When $\chi^2 = 33$, we claim that we can distinguish the spin s_a particle from the spin s_b particle at 95% CL, corresponding to the p-value of 2.5×10^{-2}, for 19 degrees of freedom (here we keep the total number of events fixed, and hence we have one degree of freedom less). The number of signal events (after reconstruction) needed to distinguish each pair of spins are listed in table 2. The same cuts as for obtaining figure 4 are applied.

In table 2, we have shown two sets of numbers. The numbers of events outside the parentheses are the minimum numbers of signal events needed to distinguish the spin for 100 fb^{-1} data. We use the same cuts as for figure 4. The number of background events is 136 with the $t\bar{t}$ dilepton events dominating (109). For reference, we also list in the parentheses the numbers of needed events assuming no background. The background distributions are canceled when comparing the observed distributions and the Monte Carlo distributions. However, they do introduce uncertainties that can significantly increase the number of needed signal events.

The numbers listed in table 2 are large but achievable in some models. For example, a KK gluon of 2 TeV in the basic RS model yields 230 events for 100 fb^{-1} in the mass window (1600 GeV, 2400 GeV), which is not enough to distinguish it from other spins at 95% CL. With 300 fb^{-1} data, we can distinguish it from a pseudo-scalar or a KK-graviton using the dilepton channel alone, but will need to combine other channels to distinguish it from a scalar.

5   Discussions and conclusions

An important assumption leading to the fully solvable system is that the only missing transverse momentum comes from the two neutrinos from the top decays. There are also

other sources of missing momenta such as neutrinos from heavy flavor hadron decays. But they are usually soft and their effects have already been included in the simulation. More challengingly, the assumption is invalid when there are other missing particles in the event, for example, in supersymmetric theories with R-parity. Consider the process $pp \to \tilde{t}\tilde{t}^* \to t\bar{t}\tilde{\chi}_1^0\tilde{\chi}_1^0$ in the minimal supersymmetric standard model, which has the same visible final state particles as a $t\bar{t}$ resonance. We have to be able to distinguish the two cases before claiming a $t\bar{t}$ resonance. Distributions in various kinematic observables are certainly different for the two cases. Nevertheless, we find that the most efficient way to separate them is still by using the event reconstruction.

As an example, we have generated 10,000 events in the above MSSM decay chain and let both t and $\bar{t}$ decay leptonically, for $m_{\tilde{t}} = 1500$ GeV and $m_{\tilde{\chi}_1^0} = 97$ GeV. There are 705 events which pass the kinematic cuts described in section 2 with a $m_{T_{\mathrm{cl}}}$ cut of 1500 GeV. Out of those 705 events, only 30 pass the reconstruction procedure, that is, satisfy eq. (2.4). This is to the vast contrast of a $t\bar{t}$ resonance of 3 TeV, where a half of the events after cuts survive the reconstruction procedure. The difference between the two cases is not difficult to understand: for a $t\bar{t}$ resonance, ignoring initial state radiations, we have t and $\bar{t}$ back-to-back in the transverse plane and their decay products nearly collinear. On the other hand, the directions of the two neutralinos in the MSSM case are unrelated and therefore the direction of the missing p_T is separated from both of the $b\ell$ systems. It is then very unlikely to satisfy the mass shell constraints simultaneously for both t and $\bar{t}$.

In conclusion, by reconstructing $t\bar{t}$ and tt events in the dilepton channel, we studied the $t\bar{t}$ and tt resonances at the LHC in a model-independent way. The kinematic system is fully solvable from the W boson and top quark mass-shell constraints, as well as the constraints from the measured missing transverse momentum. After solving this system for the momenta of the two neutrinos, we obtained the t, $\bar{t}$ momenta and therefore the $t\bar{t}$ invariant mass distribution. The same procedure can also be applied to the tt system. We showed that this method can be utilized to discover and measure the spins of $t\bar{t}$ and tt resonances at the LHC.

The event reconstruction is the most challenging when the $t\bar{t}$ resonance is heavy. This is not only because of the suppression of parton distribution functions at high energies. More importantly, in this case the top quarks are highly boosted and the lepton and the b-jet from the same top decay are highly collimated. Therefore, the lepton is often not isolated from the b-jet. To solve this problem, we included non-isolated muons, which can be identified in a detector. The b-tagging efficiency may also degrade at high energies, which drove us to consider events without b-tagged jets. In summary, we included all events with two high p_T (isolated or non-isolated) leptons and two high p_T (b-tagged or not-tagged) jets passing the kinematic cuts described in section 2.2. Accordingly, we have to consider all SM backgrounds containing the same final state particles. We simulated and analyzed all major backgrounds and found that they can be efficiently reduced by imposing the kinematic cuts and the mass-shell constraints.

The reconstruction procedure was applied to four $t\bar{t}$ resonances with different spins. We found that despite a smaller branching ratio, the dilepton channel is competitive to the semileptonic channel in discovering the $t\bar{t}$ resonance. This is due to the better experimental

resolution of the lepton momentum measurement and smaller SM backgrounds. For example, the first KK gluon in the basic RS model with fermions propagating in the bulk can be discovered at $5\,\sigma$ level or better, up to a mass of 3.7 TeV for 300 fb^{-1} integrated luminosity. We also considered the possibility of finding a $t\,t$ resonance, for which the dilepton channel is the best because it is the only channel in which the charges of both tops can be identified. Due to the smallness of the SM same-sign dilepton backgrounds, the $t\,t$ resonance has a better discovery limit than the $t\,\bar{t}$ resonance. Assuming the same production cross section as the KK gluon, the $t\,t$ resonance can be discovered up to a mass of 4.4 TeV.

The dilepton channel is also advantageous for identifying the spin of the resonance. We considered the top quark angular distribution in the $t\,\bar{t}$ rest frame, and the opening angle distribution of the two leptons in their respective top quark rest frames. Combining those two distributions, we found that for 100 fb^{-1} a few hundred signal events (after reconstruction) are needed to distinguish the spins of different resonances.

Acknowledgments

References

[1] C.T. Hill and E.H. Simmons, *Strong dynamics and electroweak symmetry breaking*, *Phys. Rept.* **381** (2003) 235 [*Erratum ibid.* **390** (2004) 553] [hep-ph/0203079] [SPIRES].

[2] C.T. Hill, *Topcolor: top quark condensation in a gauge extension of the standard model*, *Phys. Lett.* **B 266** (1991) 419 [SPIRES];
For a solution of the fine-tuning problem in the top condensation models see Y. Bai, M. Carena and E. Ponton, *The Planck scale from top condensation*, arXiv:0809.1658 [SPIRES];
C.T. Hill and S.J. Parke, *Top production: sensitivity to new physics*, *Phys. Rev.* **D 49** (1994) 4454 [hep-ph/9312324] [SPIRES].

[3] N. Arkani-Hamed, A.G. Cohen and H. Georgi, *Electroweak symmetry breaking from dimensional deconstruction*, *Phys. Lett.* **B 513** (2001) 232 [hep-ph/0105239] [SPIRES];
For a review see M. Schmaltz and D. Tucker-Smith, *Little Higgs review*, *Ann. Rev. Nucl. Part. Sci.* **55** (2005) 229 [hep-ph/0502182] [SPIRES].

[4] L. Randall and R. Sundrum, *A large mass hierarchy from a small extra dimension*, *Phys. Rev. Lett.* **83** (1999) 3370 [hep-ph/9905221] [SPIRES].

[5] Y. Nomura, D. Tucker-Smith and N. Weiner, *GUT breaking on the brane*, *Nucl. Phys.* **B 613** (2001) 147 [hep-ph/0104041] [SPIRES];
A. Pomarol, *Grand Unified Theories without the desert*, *Phys. Rev. Lett.* **85** (2000) 4004 [hep-ph/0005293] [SPIRES];
L. Randall and M.D. Schwartz, *Unification and the hierarchy from AdS$_5$*, *Phys. Rev. Lett.* **88** (2002) 081801 [hep-th/0108115] [SPIRES].

[6] K. Agashe, A. Belyaev, T. Krupovnickas, G. Perez and J. Virzi, *LHC signals from warped extra dimensions*, *Phys. Rev.* **D 77** (2008) 015003 [`hep-ph/0612015`] [SPIRES];
V. Barger, T. Han and D.G.E. Walker, *Top quark pairs at high invariant mass: a model-independent discriminator of new physics at the LHC*, *Phys. Rev. Lett.* **100** (2008) 031801 [`hep-ph/0612016`] [SPIRES];
B. Lillie, L. Randall and L.-T. Wang, *The bulk RS KK-gluon at the LHC*, *JHEP* **09** (2007) 074 [`hep-ph/0701166`] [SPIRES];
B. Lillie, J. Shu and T.M.P. Tait, *Kaluza-Klein gluons as a diagnostic of warped models*, *Phys. Rev.* **D 76** (2007) 115016 [`arXiv:0706.3960`] [SPIRES].

[7] U. Baur and L.H. Orr, *High p_T top quarks at the Large Hadron Collider*, *Phys. Rev.* **D 76** (2007) 094012 [`arXiv:0707.2066`] [SPIRES].

[8] U. Baur and L.H. Orr, *Searching for $t\bar{t}$ resonances at the Large Hadron Collider*, *Phys. Rev.* **D 77** (2008) 114001 [`arXiv:0803.1160`] [SPIRES].

[9] M. Jezabek and J.H. Kuhn, *Lepton spectra from heavy quark decay*, *Nucl. Phys.* **B 320** (1989) 20 [SPIRES].

[10] S. Willenbrock, *The standard model and the top quark*, `hep-ph/0211067` [SPIRES].

[11] R.N. Mohapatra, N. Okada and H.-B. Yu, *Diquark Higgs at LHC*, *Phys. Rev.* **D 77** (2008) 011701 [`arXiv:0709.1486`] [SPIRES].

[12] S. Bar-Shalom, A. Rajaraman, D. Whiteson and F. Yu, *Collider signals of maximal flavor violation: same-sign leptons from same-sign tops at the tevatron*, *Phys. Rev.* **D 78** (2008) 033003 [`arXiv:0803.3795`] [SPIRES].

[13] J. Gao, C.S. Li, X. Gao and Z. Li, *Same-sign top pair production in an extra-dimension model of flavor at the CERN Large Hadron Collider*, *Phys. Rev.* **D 78** (2008) 096005 [`arXiv:0808.3302`] [SPIRES].

[14] V. Simak, P. Homola, J. Valenta and R. Leitner, *Reconstruction of top-antitop system from 2 leptons and 2 jets final states in experiment ATLAS*, ATL-PHYS-2001-018.

[15] L. Sonnenschein, *Analytical solution of $t\bar{t}$ dilepton equations*, *Phys. Rev.* **D 73** (2006) 054015 [*Erratum ibid.* **D 78** (2008) 079902] [`hep-ph/0603011`] [SPIRES];

[16] H.-C. Cheng, J.F. Gunion, Z. Han, G. Marandella and B. McElrath, *Mass determination in SUSY-like events with missing energy*, *JHEP* **12** (2007) 076 [`arXiv:0707.0030`] [SPIRES].

[17] M. Davids et al., *Measurement of top-pair cross section and top-quark mass in the di-lepton and full-hadronic channels with CMS*, CMS-NOTE-2006-077.

[18] M. Beneke et al., *Top quark physics*, `hep-ph/0003033` [SPIRES].

[19] J. Thaler and L.-T. Wang, *Strategies to identify boosted tops*, *JHEP* **07** (2008) 092 [`arXiv:0806.0023`] [SPIRES].

[20] D.E. Kaplan, K. Rehermann, M.D. Schwartz and B. Tweedie, *Top tagging: a method for identifying boosted hadronically decaying top quarks*, *Phys. Rev. Lett.* **101** (2008) 142001 [`arXiv:0806.0848`] [SPIRES];
L.G. Almeida et al., *Substructure of high-p_T Jets at the LHC*, `arXiv:0807.0234` [SPIRES].

[21] S. González de la Hoz, L. March and E. Ros, *Search for hadronic decays of Z_H and W_H in the little Higgs model*, ATL-PHYS-PUB-2006-003 (2006);
L. March, E. Ros and B. Salvachúa, *Search for Kaluza-Klein excitations of the gluon in models with extra dimensions*, ATL-PHYS-PUB-2006-002 (1996).

[22] R. Frederix and F. Maltoni, *Top pair invariant mass distribution: a window on new physics*, *JHEP* **01** (2009) 047 [arXiv:0712.2355] [SPIRES].

[23] M. Arai, N. Okada, K. Smolek and V. Simak, *Top quark spin correlations in the Randall-Sundrum model at the CERN Large Hadron Collider*, *Phys. Rev.* **D 75** (2007) 095008 [hep-ph/0701155] [SPIRES].

[24] T. Han, *The "top priority" at the LHC*, *Int. J. Mod. Phys.* **A 23** (2008) 4107 [arXiv:0804.3178] [SPIRES].

[25] J. Alwall et al., *MadGraph/MadEvent v4: the new web generation*, *JHEP* **09** (2007) 028 [arXiv:0706.2334] [SPIRES].

[26] J. Pumplin et al., *New generation of parton distributions with uncertainties from global QCD analysis*, *JHEP* **07** (2002) 012 [hep-ph/0201195] [SPIRES].

[27] T. Sjöstrand, S. Mrenna and P. Skands, *PYTHIA 6.4 physics and manual*, *JHEP* **05** (2006) 026 [hep-ph/0603175] [SPIRES].

[28] J. Conway, *PGS 4, Pretty Good Simulation of high energy collisions*, http://www.physics.ucdavis.edu/∼conway/research/software/pgs/pgs4-general.htm.

[29] See for example C. Diaconu, *Structure functions*, *Int. J. Mod. Phys.* **A 24** (2009) 1069 [arXiv:0901.0046] [SPIRES].

[30] PARTICLE DATA GROUP collaboration, C. Amsler et al., *Review of particle physics*, *Phys. Lett.* **B 667** (2008) 1 [SPIRES].

[31] J.C. Collins and D.E. Soper, *Angular distribution of dileptons in high-energy hadron collisions*, *Phys. Rev.* **D 16** (1977) 2219 [SPIRES].